# Interfacial Stress Transfer in Nylon-6/E-Glass Microcomposites: Effect of Temperature and Strain Rate

ALESSANDRO PEGORETTI, LUCA FAMBRI, *and* CLAUDIO MIGLIARESI

*University of Trento*
*Department of Materials Engineering*
*Via Mesiano 77-38050, Trento, Italy*

In this study, the interfacial properties between E-glass fibers with different commercial sizings have been investigated on model composites with a nylon-6 matrix. In particular, the fiber critical length was measured by means of the single-fiber fragmentation test over a wide range of temperatures (from 25 to 175°C) and strain rates (from 0.008 to 4 $min^{-1}$). The general trend observed is that the fiber critical aspect ratio increases as the temperature increases and it decreases as strain rate is increased. The fiber critical aspect ratio for unsized fibers resulted to be reasonably well linearly related to the square root of the fiber to matrix modulus ratio. This results is in accordance with the Cox's shear-lag theoretical model and the Termonia's numerical simulations. Sized fibers display an higher deviation from the theoretical prevision probably because of the presence of interphases whose properties are different from the bulk matrix. As a consequence, the interfacial shear strength values resulted to be dependent on the fiber sizing. In particular, the fibers coated with an epoxy sizing showed a superior thermal stability of the fiber matrix-interface with respect to the unsized or nylon compatible sized fibers.

## INTRODUCTION

It is well known that mechanical performances of composite materials are strongly dependent upon the efficiency of the matrix to fiber stress transfer (1, 2). It has been proven that this process is mainly controlled by the mechanical properties of both fiber and matrix (3–9), and by the interfacial adhesion level (8, 10–13). Moreover the properties of the interphase layer near the fiber surface can be quite different from those of the bulk matrix, thus affecting the stress transfer process (6, 14–18). For any given composite material, the highest level of shear stress transferable at the fiber-matrix interface is usually called interfacial shear strength (ISS). Intensive studies have focused on the development of reliable experimental test procedures for the fiber/matrix interfacial strength measurement (19–21). The most common methods are based on micromechanical tests, performed on single fiber composites, such as the fragmentation test (22–26), the single fiber pull-out test (27, 28), the microdebond test (29–32), and microindentation test (33–35). Among them, one of the most widely studied testing methods is the "embedded single fiber" or fragmentation test. This test is performed on tensile specimens in which a single fiber is embedded in the centerline of a matrix coupon. Upon application of a tensile force, the embedded fiber breaks repeatedly in correspondence of points where the local fiber strength is reached. Continuous deformation of the specimen creates fiber fragments so short that the shear stress transfer can no longer build up enough tensile stress to cause further fiber failures. At this stage a limiting fragment size, defining a critical length $L_c$, is reached (saturation point). From the value of $L_c$ and the extrapolated fiber mean strength at the critical length, a mechanical parameter called interfacial shear strength, ISS, is usually obtained on the basis of a simplistic force equilibrium, based on the shear-lag (3) or elastic-plastic stress analyses (22). A more rigorous treatment of the fragmentation test process requires dealing with the high complexity of the interfacial stress state (21, 25, 26) and with a very careful handling of the statistic in order to avoid errors due to the extrapolation of the fiber strength to very small lengths (36–38).

Matrix mechanical properties play a major role in determining the interfacial micromechanical behavior. As a consequence, aiming at predicting the efficiency of the shear stress transfer process for many polymeric matrices their viscoelastic behavior has to be

taken into account. Nevertheless, little experimental work exists on the effect of temperature (5, 12, 38–48) and strain rate (43, 48) on the interfacial shear stress transfer process and on ISS. The purpose of this study is to investigate the effect of temperature and strain rate on the interfacial shear stress transmission efficiency and on the interfacial shear strength in nylon-6/E-glass fibers model composites. A nylon-6 matrix was chosen because it displays a marked viscoelastic behavior even at room temperature, with mechanical properties strongly dependent on both test temperature and strain rate (49). E-glass fibers were selected on the basis of their extremely extended use as reinforcing materials in nylon-6 matrix composites (49).

## EXPERIMENTAL

### Materials

The matrix of the microcomposites used in this work was a cast nylon-6 film (SNIA S.p.A., Italy) with a nominal thickness of 45 μm. Films were dried under vacuum at 100°C for 48 h, and then stored under vacuum in a desiccator until use.

The following E-glass fibers were used as-received:

- "Sisecam unsized" (Sisecam, Turkey), nominal diameter 14 μm, unsized;
- "Sisecam PA-sized" (Sisecam, Turkey), nominal diameter 14 μm, surface treated with a commercial polyamide compatible coupling agent;
- "PPG EP-sized" (PPG, The Netherlands, trade name Hybon 2001), nominal diameter 24 μm, surface treated with a commercial epoxy compatible coupling agent.

Direct information on the sizing chemical composition was not available from the producers.

Sized fibers were used as received, whereas unsized fibers were carefully washed in acetone and dried before sample preparation.

### Sample Preparation

Microcomposite samples were obtained by compression molding with an experimental setup assembled as in *Fig. 1a*. In particular, about 15 fibers were carefully aligned within two nylon-6 films sandwiched between two PTFE sheets (thickness of 0.5 mm) and two aluminum plates. The mold was placed in an oven under vacuum at a temperature of 290°C and at a pressure of about 7 kPa for about 45 min and then it was cooled in air. Samples were obtained by cutting strips containing one single fiber longitudinally aligned in the centerline, as depicted in *Fig. 1b*. The thickness of the microcomposites was about 85–90 μm for all cases. Before testing, all samples were exposed at the laboratory conditions (T≈20°C, R. H.≈50%) till a constant weight was reached, which usually occurred after about one week (see *Fig. 2*).

### Material Characterization

The mechanical properties of the nylon-6 matrix were determined by tensile tests performed on two layer samples prepared by the same compression molding process as for the single fiber composites. Tensile tests were performed on strip samples with a gauge length of 25 mm, by using an Instron 4502 tensile tester equipped with a 100 N load cell and a thermostatic chamber (Instron model 3119). Tests were done at various strain rates in the range 0.008–4 $min^{-1}$, and various temperatures from 25 to 175°C.

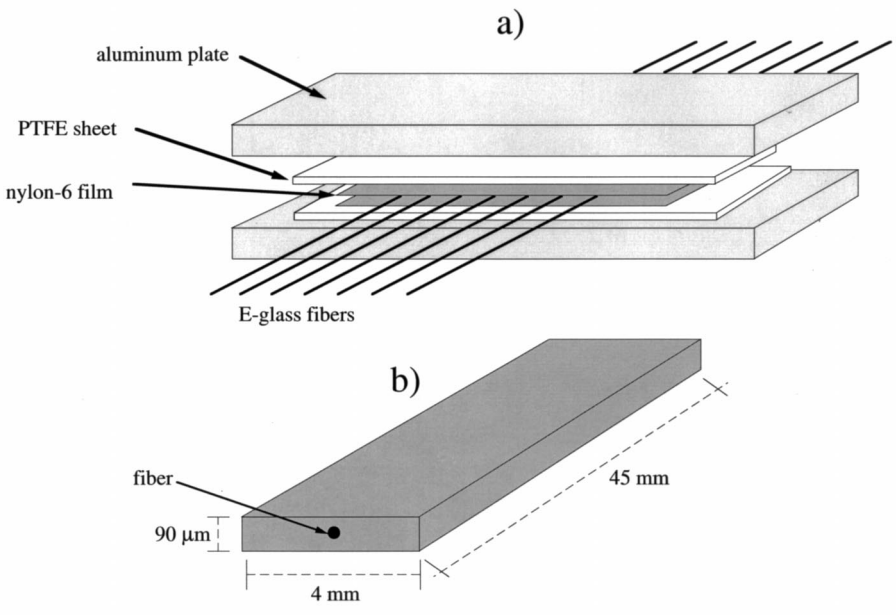


*Fig. 1. Schematic illustration of a) the compression molding set for the preparation of single fiber model composites, and b) geometry and dimensions of the single fiber specimens.*

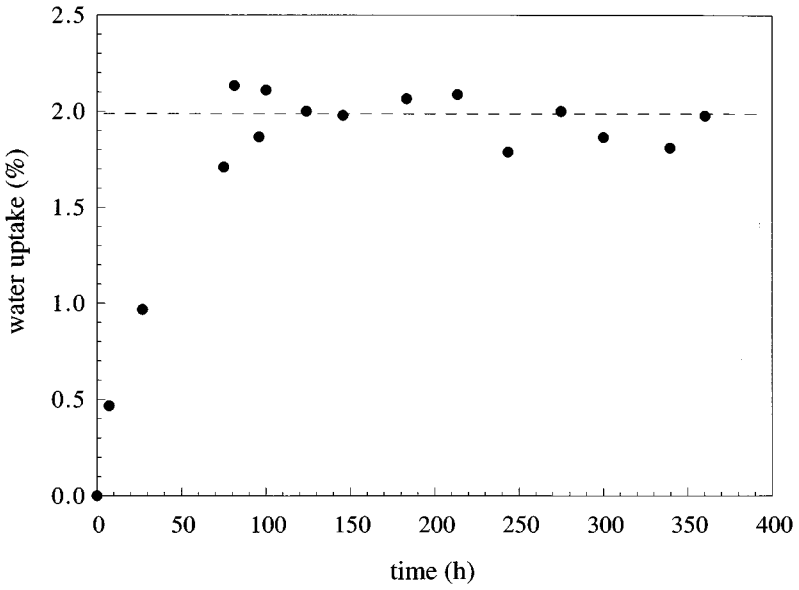


*Fig. 2. Water uptake during exposure at laboratory conditions for a molded single fiber specimen.*

Differential scanning calorimetry (DSC) measurements were performed by a Mettler DSC 30 apparatus, at a heating rate of 10°C $min^{-1}$, under a nitrogen flux of 10 ml $min^{-1}$ in the temperature range 0–260°C. The dry compression molded samples showed a glass transition temperature of 42°C, and a melting temperature of 221°C. The crystallinity percentage, $X_c$, was assessed by integrating the normalized area of the endothermal peak, and rating the heat involved to the reference value of the 100% crystalline polymer, i.e. 190 J/g (50), thus obtaining a value of about 22% by weight.

Fiber tensile stress and strain at break were measured at various gauge lengths on monofilaments randomly extracted from a bundle. According to the ASTM standard D3379-75, a single fiber was centerline-mounted on window cards using a quick-setting glue and tested at room temperature and at a crosshead speed of 0.2 mm $min^{-1}$ using the Instron machine equipped with a 10 N load cell. Sisecam fibers were tested at gauge lengths of 5, 10, 15, 20 and 25 mm, while PPG EP-sized fibers were tested at gauge lengths of 5, 10, 20, 25 and 40 mm. Strain at break values were corrected to account for the compliance of the measuring system. Weibull shape, $\alpha$, and scale, $\beta$, parameters (36) were determined on the basis of an iterative procedure proposed by Gurvich *et al.* (38). The average strength $\bar{\sigma}_{fb}(L)$ at an arbitrary length L may then be estimated as:

$$\bar{\sigma}_{fb}(L) = \alpha\left(\frac{L}{L_0}\right)^{-1/\beta}\Gamma\left(1+\frac{1}{\beta}\right) \qquad (1)$$

where $L_0$ is the reference length and $\Gamma$ is the gamma function.

The chemical composition of the fiber surface was investigated by means of X-ray photoelectron spectroscopy (XPS). Measurements were performed with a Perkin Elmer PHI 5500 ESCA System, using an aluminum anode working at 14 kV (power of 200 W). The pressure in the vacuum chamber was set at about $10^{-8}$ Pa. Samples of multifilament fiber were analyzed in an area of 400 micron diameter; the sampling depth was about 5 nm. Curve fitting and quantification of elements were accomplished using the software and sensitivity factors supplied by the manufacturer. In high-resolution spectra, all binding energies were referenced by setting the CHx peak maximum in the resolved C1s spectra to 285 eV. The reported data are an average of measurements performed in three different zones.

## Fragmentation Test

Fragmentation experiments were performed, at various temperatures (from 25 to 175°C) and strain rates (from 0.008 to 4 $min^{-1}$), by using the custom-made apparatus schematically represented in *Fig. 3*. This device consists of a small tensile tester (Minimat, by Polymer Laboratories), equipped with a thermostatic chamber, and put under a polarized optical stereo-microscope (Wild M3Z by Leica). At least five samples were tested for each experimental condition. All samples were loaded up to a strain of 20% in order to ensure the saturation of the fragmentation process. The mean fiber length, $\bar{L}_s$, was measured by means of an image analyzer system, and, as proposed by Ohsawa *et al.* (39), the fiber critical length, $L_c$, was considered equal to (4/3) $\bar{L}_s$. The interfacial shear strength (ISS) was evaluated following the simplified physical model proposed by Kelly and Tyson (22), which yields the well-known expression:

$$ISS = \frac{\bar{\sigma}_{fb}(L_c)\, d}{2L_c} \qquad (2)$$

where $\bar{\sigma}_{fb}$ ($L_c$) is the mean fiber strength at the critical length.

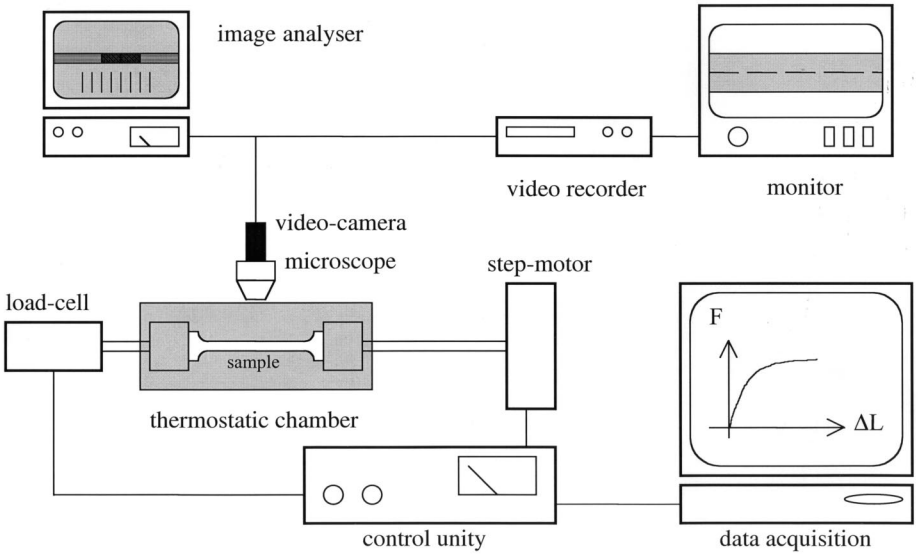


*Fig. 3. Schematic of the experimental apparatus for the single fiber fragmentation test.*

## RESULTS AND DISCUSSION

The strength parameters experimentally measured on the E-glass fibers used in this work are reported in *Table 1*. It is worth noting that unsized fibers show lower values of the Weibull scale parameter with respect to both sized fibers.

Preliminary mechanical measurements on the pure matrix evidenced that, as reported in *Figs. 4* and *5*, both tensile modulus ($E_m$) and yield strength ($\sigma_y$) are strongly influenced by temperature and strain rate variations. As expected (49), both $E_m$ and $\sigma_y$ are decreasing as temperature increases, while they increase as strain rate increases. These viscoelastic effects are particularly pronounced because the glass transition temperature of the saturated PA6 matrix is quite close to room temperature, being located at about 42°C (from DSC measurement).

Results of fragmentation experiments performed on single fiber composites at various temperatures from 25 to 175°C are presented in *Fig. 6*. As observed by other authors (5, 12, 39–48) the critical fiber aspect ratio defined as the ratio between the fiber critical length ($L_c$) and the fiber diameter (d) increases as the temperature increases. On the other hand, as can be observed in *Fig. 7*, the effect of an increase in the strain rate is to reduce the fiber critical aspect ratio. It is worth noting that the authors previously reported similar effects on low $T_g$ (39°C) epoxy matrix model composites reinforced with carbon fibers (43). As the fiber critical aspect ratio is related to the fiber/matrix stress transfer it is evident that both temperature and strain rate markedly influence the efficiency of the shear stress transfer process. From a theoretical point of view the interfacial stress transfer process can be analyzed by the classical shear lag theory, proposed by Cox (3). On the basis of Cox's analysis the critical aspect ratio, $\frac{L_c}{d}$, can be related to the ratio of fiber to matrix elastic modulus, $\frac{E_f}{E_m}$, through the following relationship:

$$\mathrm{Log}\left(\frac{L_c}{d}\right) \approx k + \frac{1}{2}\,\mathrm{Log}\left(\frac{E_f}{E_m}\right) \qquad (3)$$

**Table 1. Single-Fiber Strength Parameters.**

| Fiber | Sisecam Unsized | Sisecam PA-Sized | PPG EP-Sized |
|---|---|---|---|
| Sizing | none | PA compatible | epoxy compatible |
| Diameter (μm) | 14 | 14 | 24 |
| Strain at break (%) for L = 25 mm (number of specimens) | 2.53 ± 0.88 (47) | 3.76 ± 0.66 (66) | 3.79 ± 0.97 (50) |
| Weibull's scale parameter α (MPa) for $L_0$ = 5 mm (number of specimens) | 1995 (158) | 2798 (167) | 3020 (133) |
| Weibull's shape parameter β | 4.010 | 6.255 | 3.934 |

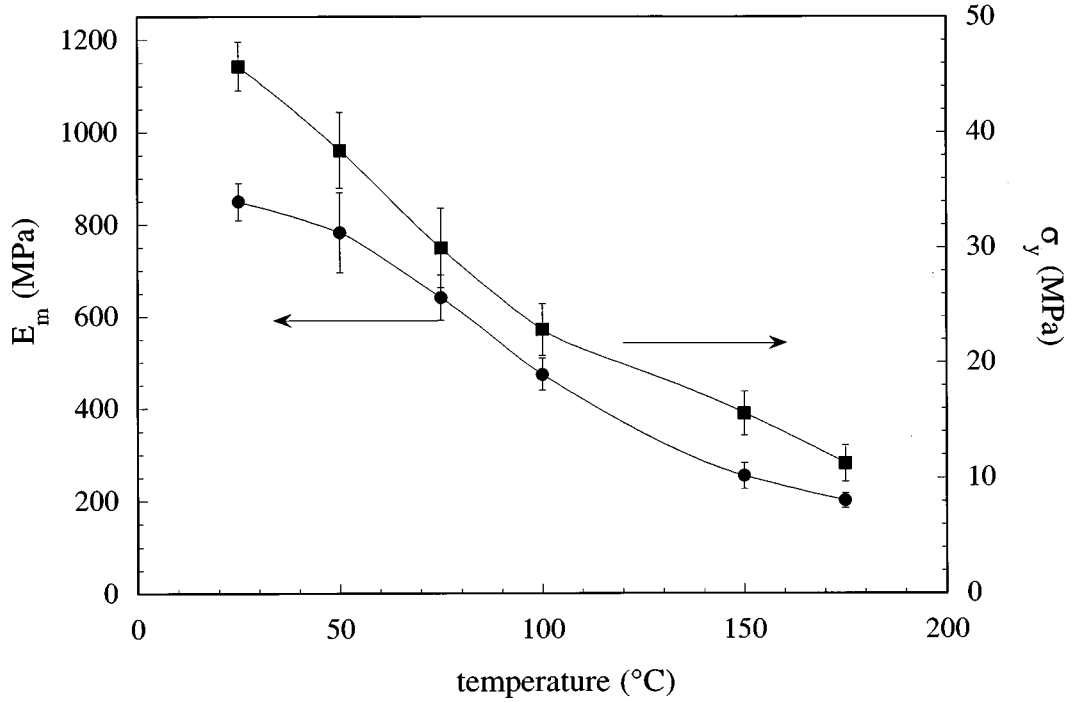


*Fig. 4. Matrix tensile modulus (●) and strength (■) as a function of temperature at a constant strain rate of 0.008 min$^{-1}$.*

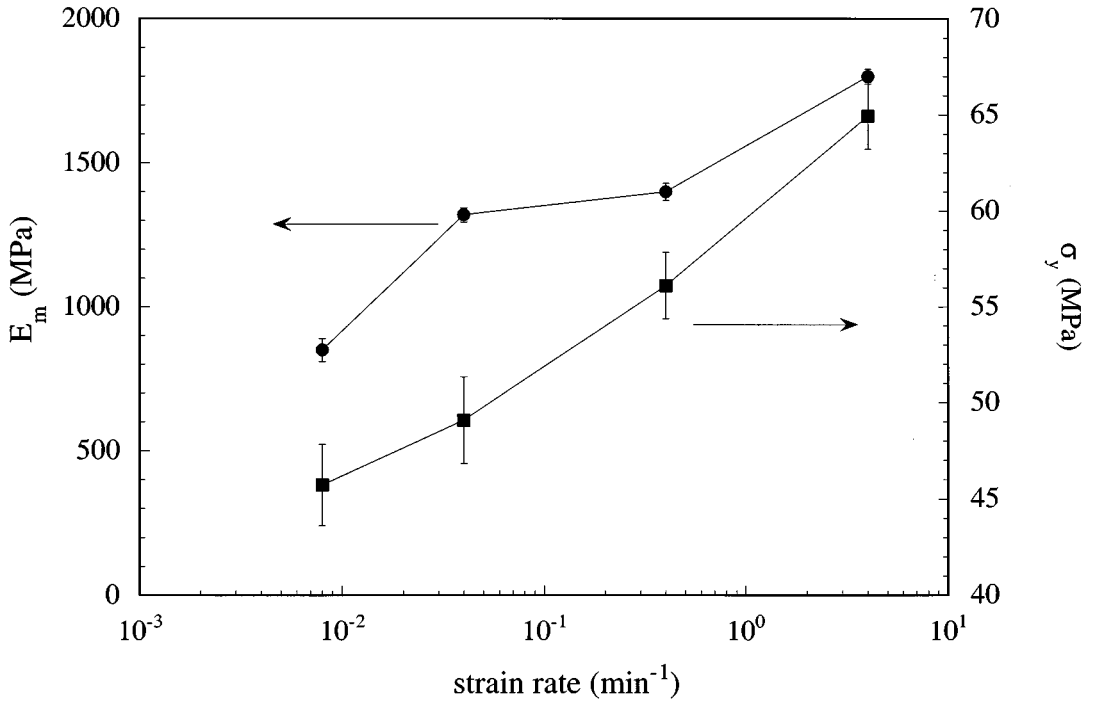


*Fig. 5. Matrix tensile modulus (●) and strength (■) as a function of strain rate at a constant temperature of 25°C.*

Cox's analysis neglects the adhesion across the end faces of the fibers and does not take into account local stress concentration effects near fiber ends. This explains why, using a finite difference technique, Termonia (4, 9) found that the dependence of $\frac{L_c}{d}$ on the ratio of fiber to matrix elastic muduli is linear in the range $\frac{E_f}{E_m} < 20$, when stress transfer mainly occurs through tensile loading across fiber ends. However, at higher $\frac{E_f}{E_m}$ values, Termonia's numerical simulation (9)

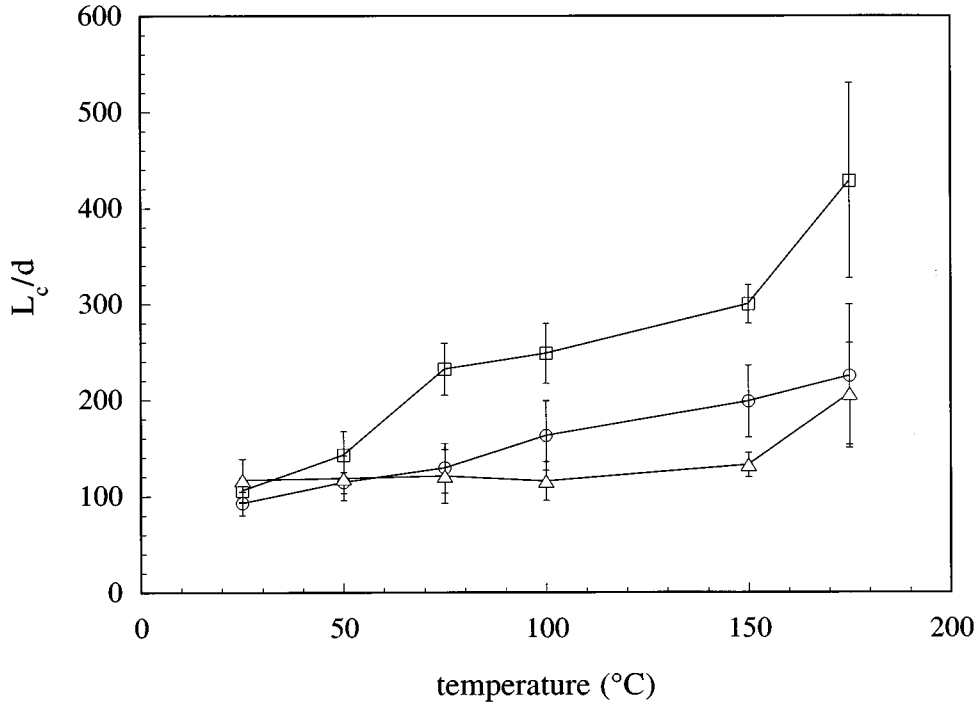


*Fig. 6. Fiber critical aspect ratio, $\frac{L_c}{d}$, as a function of temperature at a constant strain rate of 0.008 min$^{-1}$, for (○) Sisecam unsized, (□) Sisecam PA-sized, and (△) PPG EP-sized glass fibers.*

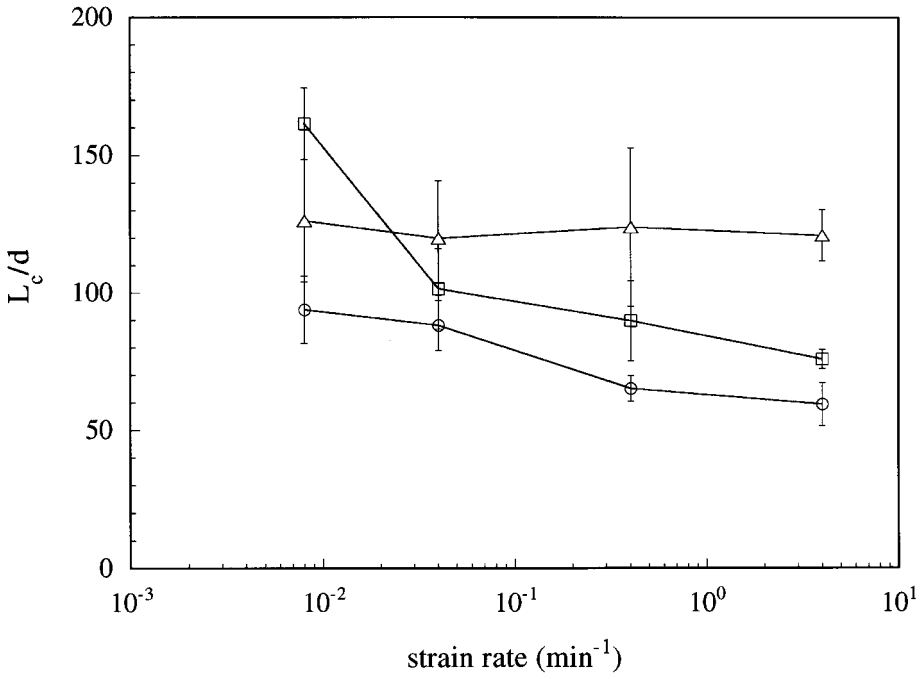


*Fig. 7. Fiber critical aspect ratio, $\frac{L_c}{d}$, as a function of strain rate at a constant temperature of 25°C, for (○) Sisecam unsized, (□) Sisecam PA-sized, and (△) PPG EP-sized glass fibers.*

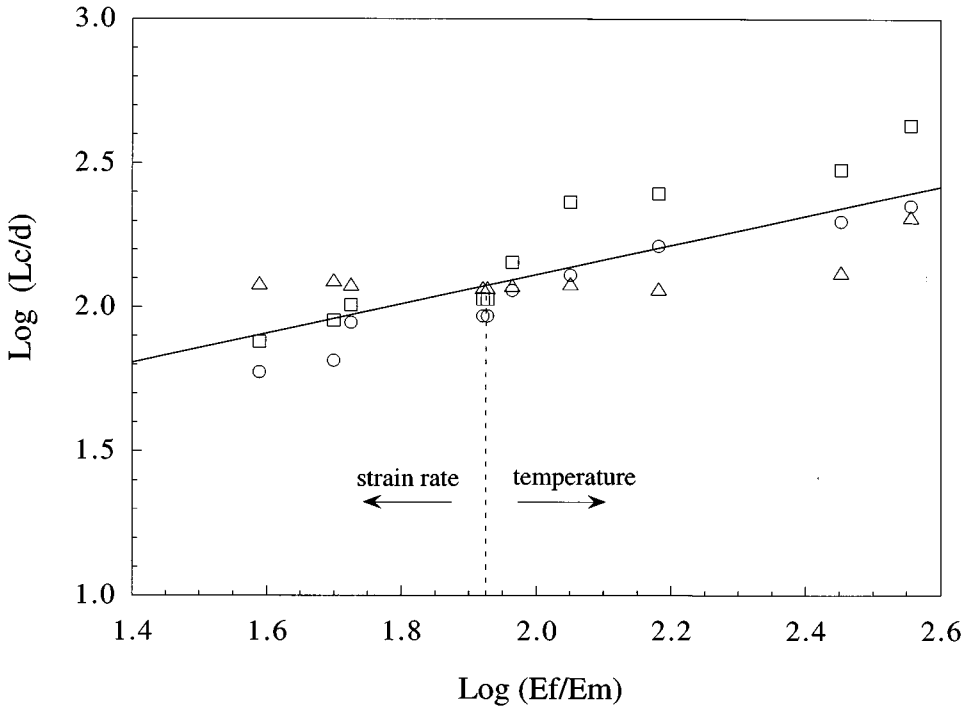


*Fig. 8. Dependence of fiber critical aspect ratio, $\frac{L_c}{d}$, on the tensile modulus ratio of fiber to matrix material, $\frac{E_f}{E_m}$. Experimental data refer to (○) Sisecam unsized, (□) Sisecam PA-sized, and (△) PPG EP-sized glass fibers. The straight line represents the linear regression on the experimental data.*

follows the predictions of the Cox's shear-lag analysis (3). It is important to observe that both Cox's model and Termonia's analysis are based on the hypothesis of perfect adhesion between fiber and matrix.

Experimental values of fiber critical aspect ratio as a function of the fiber to matrix elastic modulus ratio are shown in *Fig. 8*, which displays how the fiber critical aspect ratio increases as $\frac{E_f}{E_m}$ increases. It is worth to remember that values of $\frac{E_f}{E_m}$ in the range from about 40 to 350 were reached by changing temperature and/or strain rate in order to obtain matrix modulus values ranging from 200 to 1800 MPa. The least squares best fit line evaluated on all the experimental data has a slope equal to 0.51 ± 0.07. This value agrees very well with the theoretical value of 0.5 predicted by Cox's shear lag analysis and Termonia's numerical simulation at $\frac{E_f}{E_m} > 20$. Nevertheless, a more detailed analysis of the data evaluated for the various fibers put in evidence slope values depending on the fibers' sizing. In particular, values of 0.78 ± 0.08 for the Sisecam PA-sized fibers, 0.60 ± 0.05 for the Sisecam PA-sized fibers, and 0.16 ± 0.06 for the PPG EP-sized fibers were found.

The effect of temperature and strain rate on the interfacial shear strength, ISS, values evaluated through *Eq 2* are reported in *Fig. 9* for all the systems under investigation. The matrix shear strength, $\tau_m$, values reported on the same graph were estimated through the Von Mises relationship, $\tau_m = \frac{\sigma_m}{\sqrt{3}}$, where $\sigma_m$ is the matrix tensile strength. Room temperature measurements evidenced a slightly higher ISS value for the Sisecam PA sized fibers. It is interesting to observe that for both unsized and PA-sized Sisecam fibers ISS values are decreasing quite rapidly as the test temperature exceeds the matrix $T_g$. On the contrary, ISS values for the PPG EP-sized fibers are rather stable as the temperature increases and they drop only when the test temperature is higher than about 120°C. It is interesting to observe that for temperatures higher than 100°C the measured values of the interfacial shear strength are even superior than the estimated matrix shear strength. This behavior suggests the existence of interphases whose properties depend on the fiber sizing. At this regard, some useful information can be obtained from the XPS data. The results reported in *Table 2* evidence the different chemical composition of the surface of the three fibers. The Sisecam unsized fibers reveal the typical E-glass components and the presence of some hydrocarbon products that probably contaminated the surface before XPS analysis. On the other hand, both PA- and EP-sized fibers exhibit a reasonable reduction of the silicon percentage and a higher percentage of carbon, due to the sizing

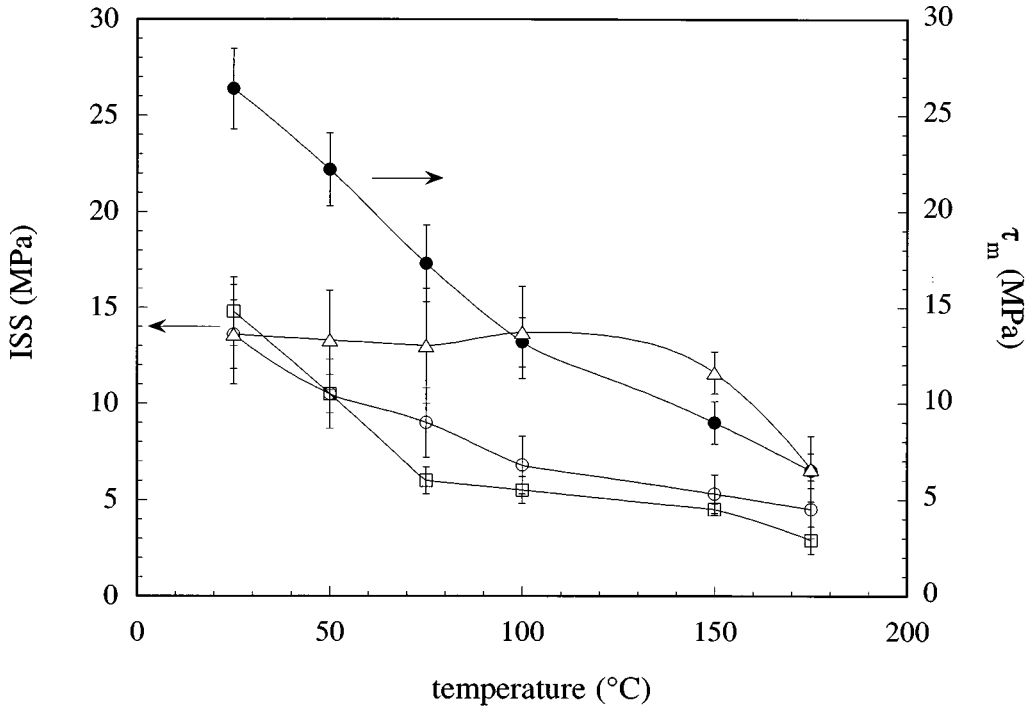


*Fig. 9. Interfacial shear strength, ISS, values* $\frac{L_c}{d}$, *as a function of temperature at a constant strain rate of 0.008 min*$^{-1}$, *for (○) Sisecam unsized, (□) Sisecam PA-sized, and (△) PPG EP-sized glass fibers. The temperature dependence of the matrix shear strength,* $\tau_m$ *(●), is also reported.*

agent that covers the glass surface. Moreover, some important differences between the two sized fibers can be evidenced. In fact, carbon and oxygen were found on both fibers, whereas only Sisecam PA-sized fibers showed the presence of nitrogen. In particular, the high resolution analysis of the C1s peak in the case of PPG EP-sized fibers showed the presence of two components at about 285 eV (corresponding to C–C and C–H bonds) and at 286.5 eV (C–O), typical of aliphatic and ether groups. In the case of PA-sized fibers, a third component at about 288.5 eV, which is typical of amide group (O=C–N), was also revealed, as confirmed by the signal of N1s at about 399 eV. On the basis of the above reported observations it is possible to assert that the sizing agent of Sisecam PA-sized probably contains amide groups and it is compatible with the nylon 6 matrix. In the case of PPG EP-sized fibers, the sizing does not contain nitrogen and hence it is very probably epoxy terminated, being the sizing specific for epoxy resins. In order to confirm this hypothesis, a reaction with perchloric acid solution in glacial acetic acid in the presence of tetraethylammonium bromide, according to ASTM D1652-90, was performed. This chemical test clearly evidenced the presence of the epoxy group. The almost constancy of ISS in the case of PPG EP-sized fibers, up to about 140°C, could be explained by the hypothesis of a chemical reaction between the epoxy group of the sizing and the amine groups of the matrix with the formation of an epoxydic interphase, whose glass transition temperature could be in the range 120–170°C. In order to confirm this supposition, further experimental work is in progress.

The strain rate dependence of the ISS shown in *Fig. 10* is consistent with the above hypothesis. In fact ISS values of the unsized and PA-sized fibers show a similar behavior, with increasing values as the strain rate increases. The trend is very similar to the observed

**Table 2. Fiber Surface Composition From XPS Analysis.**

| | Atomic Composition (%) | | | | | | | | | |
|---|---|---|---|---|---|---|---|---|---|---|
| Fiber | C | O | Si | N | A1 | Mg | P | Ca | C1 | B |
| Sisecam unsized | 47.2 | 30.4 | 15.1 | | 1.9 | 0.9 | 1.2 | 0.9 | 1.2 | 1.0 |
| Sisecam PA-sized | 67.2 | 24.4 | 2.9 | 3.9 | 0.5 | | | 0.4 | | 0.7 |
| PPG EP-sized | 73.7 | 23.4 | 2.4 | | 0.4 | | | | | |

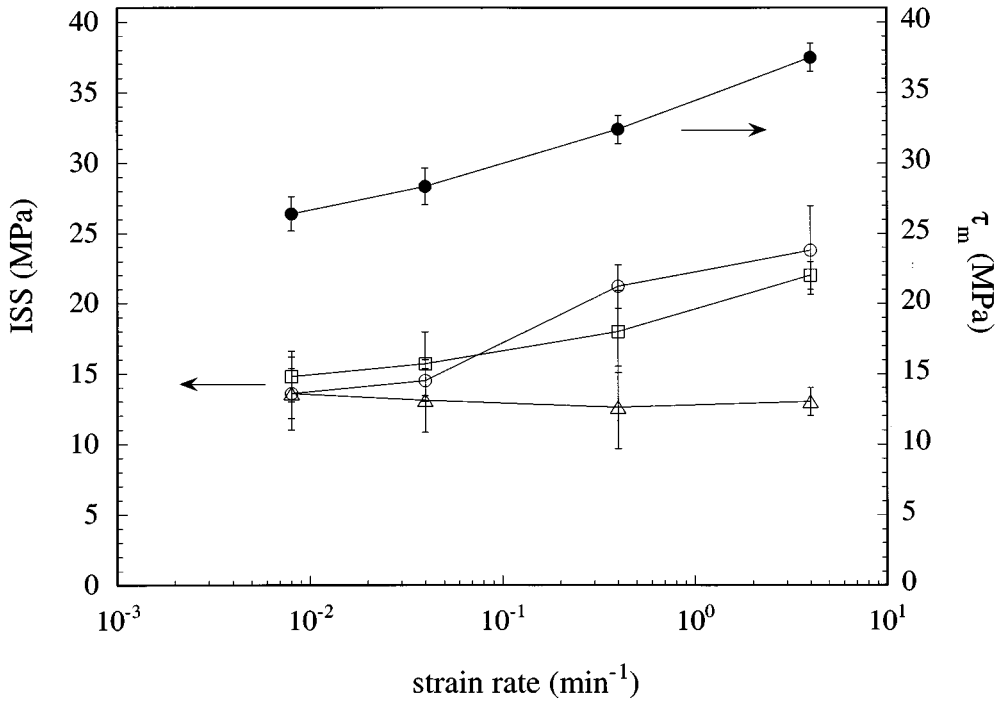


*Fig. 10. Interfacial shear strength, ISS, values* $\frac{L_c}{d}$, *as a function of strain rate at a constant temperature of 25°C, for (○) Sisecam unsized, (□) Sisecam PA-sized, and (△) PPG EP-sized glass fibers. The strain rate dependence of the matrix shear strength,* $\tau_m$ *(●), is also reported.*

matrix shear strength increase. On the contrary, ISS values for the PPG EP-sized fibers do not appreciably change as the strain rate increases, thus suggesting the existence of an interphase with an higher glass transition temperature and reduced viscoelastic effects at room temperature.

In the light of the above reported considerations it is now interesting to reconsider the data reported in *Fig. 8*. The linear regression line of the fiber critical length values for the PPG EP-sized fibers has a slope significantly lower (0.16) than the theoretical value of 0.5. This is probably due to the presence of an interphase whose elastic modulus is less sensitive to changes in either temperature and strain rate than the bulk matrix. On the other hand, the higher slope value obtained for the Sisecam PA-sized fibers (0.78) could be related to the presence of an intherphase whose stiffness is lower than that of the pure matrix.

## CONCLUSIONS

The temperature and strain rate dependence of the fiber critical length was investigated for various E-glass/nylon-6 model composites by means of the single fiber fragmentation test. The method was found to provide useful information for understanding fiber/matrix interactions. Results show that the fiber critical aspect ratio increases as the temperature increases and decreases as strain rate is increased. Temperature and strain rate cause strong variation of the matrix mechanical properties because of its pronounced viscoelastic nature. In good accordance with both Cox's theoretical model and Termonia's numerical simulations, fiber critical aspect ratio values for unsized fibers were found to be linearly related to the square root of the fiber to matrix modulus ratio.

Interfacial shear strength values were found to be strictly dependent on the fiber surface sizing. In particular, a higher thermal stability of the fiber/matrix interface was achieved in the case of the fiber coated with a sizing for epoxy resin. This result was tentatively explained by supposing the existence of an interphase with reduced viscoelastic effects at room temperature.

## ACKNOWLEDGMENTS

This work was partially supported by Consiglio Nazionale delle Ricerche, CNR, Roma. The authors would like to thank Mr. L. Menaldo for carrying out most of the experimental work, and Dr. M. Morra (Nobilbioricerche, Asti, Italy) for XPS analysis.

## REFERENCES

1. P. Yeung and L. J. Broutman, *Polym. Eng. Sci.*, **18**, 62 (1978).
2. M. S. Madhukar and L. T. Drzal, *J. Compos. Mater.*, **25**, 932 (1991); *J. Compos. Mater.*, **25**, 958 (1991); *J. Compos. Mater.*, **26**, 310 (1992); *J. Compos. Mater.*, **26**, 936 (1992).
3. H. L. Cox, British, *J. Appl. Phys.*, **3**, 72 (1952).

4. Y. Termonia, *J. Mat. Sci.*, **22**, 504 (1987).
5. El. M. Asloun, M. Nardin, and J. Schultz, *J. Mat. Sci.*, **24**, 1835 (1989).
6. V. Rao and L. T. Drzal, *Polym. Comp.*, **12**, 48 (1991).
7. V. Rao and L. T. Drzal, *J. Adhesion*, **37**, 83 (1992).
8. L. Monette, M. P. Anderson, S. Ling, and G. S. Grest, *J. Mat. Sci.*, **27**, 4393 (1992).
9. Y. Termonia, *J. Mat. Sci. Letters*, **12**, 732 (1993).
10. L. T. Drzal, M. J. Rich, and P. F. Lloyd, *J. Adhesion*, **16**, 1 (1982).
11. W. A. Fraser, F. H. Ancker, A. T. DiBenedetto, and B. Elbirli, *Polym. Comp.*, **4**, 238 (1983).
12. A. T. DiBenedetto and P. J. Lex, *Polym. Eng. Sci.*, **29**, 543 (1989).
13. B. Harris, O. G. Braddell, C. Lefebvre, and J. Verbist, *Plas. Rub. Comp. Proc. and Appl.*, **18**, 221 (1992).
14. L. T. Drzal, "The interphase in epoxy composites," in *Advances in Polymer Science, 75: Epoxy Resins and Composites II*, pp. 1–32, K. Dusek, Springler Verlag, Berlin (1985).
15. W. S. Carvalho and R. E. S. Bretas, *Eur. Polym. J.*, **7**, 817 (1990).
16. Y. Termonia, *J. Mat. Sci.*, **25**, 103 (1990).
17. S. Incardona, C. Migliaresi, H. D. Wagner, A. H. Gilbert, and G. Marom, *Comp. Sci. & Techn.*, **47**, 43 (1993).
18. T. H. Cheng, J. Zhang, S. Yumitori, F. R. Jones, and C. W. Anderson, *Composites*, **25**, 661 (1994).
19. P. J. Herrera-Franco and L. T. Drzal, *Composites*, **23**, 2 (1992).
20. M. Narkis and J. H. Chen, *Polym. Comp.*, **9**, 245 (1988).
21. J.-K. Kim and Y.-W. Mai, *Engineered Interfaces in Fiber Reinforced Composites*, Elsevier Science Ltd., Oxford, U.K. (1998).
22. A. Kelly and W. R. Tyson, *J. Mech. Phys. Solids*, **13**, 329 (1965).
23. A. A. Fraser, F. H. Ancker, and A. T. DiBenedetto, Proc. 30th SPI RP/C Conf., Sec. 22-A (1975).
24. A. T. DiBenedetto, *Comp. Sci. & Techn.*, **42**, 103 (1991).
25. P. Feillard, G. Désarmont, and J. P. Favre, *Comp. Sci. & Techn.*, **49**, 109 (1993).
26. P. Feillard, G. Désarmont, and J. P. Favre, *Comp. Sci. & Techn.*, **50**, 265 (1994).
27. L. J. Broutman, *ASTM STP*, **452**, 27 (1969).
28. L. S. Penn and S. M. Lee, *J. Comp. Techn. & Res.*, **11**, 23 (1989).
29. P. S. Chua and M. R. Piggot, *Comp. Sci. & Techn.*, **22**, 33 (1985).
30. B. Miller, P. Muri, and L. Rebenfeld, *Comp. Sci. & Techn.*, **28**, 17 (1987).
31. U. Gaur and B. Miller, *Comp. Sci. & Techn.*, **34**, 35 (1989).
32. H. D. Wagner, H. E. Gallis, and E. Wiesel, *J. Mat. Sci.*, **28**, 2238 (1993).
33. J. F. Mandell, D. H. Grande, T. H. Tsiang, and F. J. McGarry, in Proc. 7th Conference *Composite Materials Testing and Design*, ASTM STP 893, pp. 87–108, J. M. Whithney, ed., Philadelphia (1986).
34. M. Desaenger and I. Verpoest, *Comp. Sci. & Techn.*, **48**, 215 (1993).
35. G. Kalinka, A. Leistner, and A. Hampe, *Comp. Sci. & Techn.*, **57**, 845 (1997).
36. W. Weibull, *J. Appl. Mech. ASME*, **18**, 293 (1951).
37. El. M. Asloun, J. B. Donnet, G. Guilpan, M. Nardin, and J. Schultz, *J. Mat. Sci.*, **24**, 3504 (1989).
38. M. R. Gurvich, A. T. DiBenedetto, and A. Pegoretti, *J. Mat. Sci.*, **32**, 3711 (1997).
39. T. Ohsawa, A. Nakayama, M. Miwa, and A. Hasegawa, *J. Appl. Polym. Sci.*, **22**, 3203 (1978).
40. A. S. Wimolkiatisak and J. P. Bell, *Polym. Comp.*, **10**, 162 (1989).
41. N. Ogata, H. Yasumoto, K. Yamasaki, H. Yu, T. Ogihara, T. Yanagawa, K. Yoshida, and Y. Yamada, *J. Mat. Sci.*, **27**, 5108 (1992).
42. T. P. Skourlis and R. L. McCullough, *Comp. Sci. & Techn.*, **49**, 363 (1993).
43. M. Detassis, A. Pegoretti, and C. Migliaresi, *Comp. Sci. & Techn.*, **53**, 39 (1995).
44. A. Pegoretti, C. Della Volpe, M. Detassis, and C. Migliaresi, *Composites*, **27A**, 1067 (1996).
45. V. K. Raghavendran, M. C. Waterbury, V. Rao, and L. T. Drzal, *J. Adhesion Sci. Technol.*, **11**, 1501 (1997).
46. P. C. Varelidis, R. L. McCullough, and C. D. Papaspyrides, *Comp. Sci. & Techn.*, **58**, 1487 (1998).
47. M. H. Auvray, P. Chéneau-Henry, F. H. Leroy, and J. P. Favre,. *Composites*, **25**, 776 (1994).
48. A. Straub, M. Slivka, and P. Schwartz, *Comp. Sci. & Techn.*, **57**, 991 (1997).
49. M. I. Kohan, *Nylon Plastics Handbook*, Hanser Publishers, Munich (1995).
50. R. Pflüge, in *Polymer Handbook*, 3rd Edition, V/112, J. Brandrup and E. H. Immergut, eds., John Wiley & Sons, New York (1989).